Available online at www.sciencedirect.com
ScienceDirect
Journal of Sound and Vibration 302 (2007) 699–715
JOURNAL OF SOUND AND VIBRATION
www.elsevier.com/locate/jsvi

Influence of frequency-dependent properties on system identification: Simulation study on a human pelvis model

N.E. Conza, D.J. Rixen*

Section Engineering Dynamics, Department of Precision and Microsystems Engineering, Faculty of Mechanical, Maritime and Materials Engineering, Delft University of Technology, Mekelweg 2, 2628CD Delft, The Netherlands

Received 16 December 2005; received in revised form 30 November 2006; accepted 30 November 2006
Available online 30 January 2007

Abstract

The experimental identification of systems in structural dynamics is commonly achieved by adapting a parametric model so that its simulated response matches a set of measurements. Since in most applications the system mechanical properties are considered constant, standard identification tools assume the same. The question arises over the identifiability of systems which do not satisfy this assumption. The objective of this simulation study is to investigate the influence of frequency-dependent stiffness and damping properties on the system identification, as performed by two standard modal analysis tools and one in-house updating algorithm. Results indicated that the frequencies and the mode shapes are generally well estimated, while the damping ratios proved more difficult to be identified.

1. Introduction

Structural dynamics is an important aspect in fields such as civil, aerospace and mechanical engineering. In order to facilitate dynamic simulation and testing, computer models are constructed and validated with respect to real measurements. One common assumption of such models is their constant mechanical properties (mass, stiffness and viscous damping) in the operation range of interest. Most standard identification tools use therefore models which satisfy the same assumption.

System identification is gaining importance also in the field of biomedical engineering. The same theories and methods are used on systems which are of biological nature. In the frame of an ongoing research on Low Back Pain, the biological system under investigation is the human pelvis. The bones composing the pelvic girdle are the two ilia and the sacrum, and they interface at the sacroiliac joints and at the symphysis pubis, as illustrated in Fig. 1. A massive ligament network holds the bony structure together.

The rationale behind this research project, which has been hypothesized and investigated in previous works [1,2] but which is still controversial, is that abnormal biomechanical properties of the sacroiliac joints can generate pain. Responding to the lack of objective diagnostics in this matter, the main goal of this research is

*Corresponding author. Tel.: +31 15 278 1523; fax: +31 15 278 2150.
E-mail address: d.j.rixen@tudelft.nl (D.J. Rixen).

0022-460X/$ - see front matter © 2007 Elsevier Ltd. All rights reserved.
doi:10.1016/j.jsv.2006.11.033

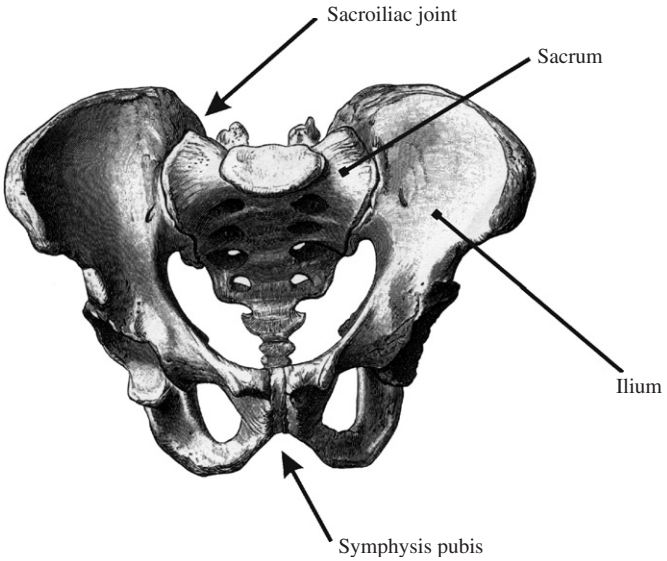

Fig. 1. Human pelvic girdle comprising the sacrum and the iliac bones. The sacrum is braced between the iliac bones at the sacroiliac joints, and the iliac bones are joined at the front at the symphysis pubis.

the development of a diagnostic tool for an objective non-invasive measurement of those properties, comprising an apparatus for the bone vibration measurements by ultrasound [3,4] and an updating algorithm to process the measurements.

A dynamic model of the human pelvis has been built to support the identification of the biomechanical properties of the sacroiliac joints. A first updating algorithm in frequency domain has been developed and tested in simulations [5].

The properties of the human pelvis have so far been modelled as constant. However, literature shows that the response of ligaments under quasi-static tensile experiments varies with the speed at which the strain or stress is imparted [6]. This suggests that the mechanical properties of ligaments might depend on the frequency of the excitation as well.

The system has been investigated by means of modal testing on fresh-frozen human specimens [7,8], in order to obtain information for the validation of the model. The validated model will then serve as a base for the updating algorithm. The question on the influence of frequency dependency is therefore relevant for the accuracy of both the modal analysis and the dedicated updating algorithm.

Fig. 2 provides an example of the typical *in vitro* response by showing drive point measurements at different times throughout one of the cadaver experiment session [8]. Based on these test data it is difficult to fully assume or rule out the possibility that there is some frequency dependency involved. On the contrary, nonlinear effects have been excluded in the measured frequency range and level of excitation by prior checks of the response at different amplitudes. The justification of this study is to assess the level of misinterpretation that can be made when analysing the response of frequency-dependent systems with standard modal analysis tools. This assessment should be made before attempting an interpretation of the real test data. With this goal in mind, the most observable system is a simulated one, where the mechanical properties are positively known. All other test benches are subject to the imprecision and uncertainty of real measurements and real system identification.

In this study the influence that a frequency dependency in the mechanical properties might have on the identification quality is investigated. Measurement data are synthesized from a model showing linear frequency-dependent stiffness, and a hysteretic damping component next to the viscous damping. In this model the elastic and dissipative forces increase with the frequency. The generated data are used as input for two standard modal analysis tools and the in-house updating algorithm. For comparison, the identification capability of the latter is evaluated with and without built-in frequency dependency.

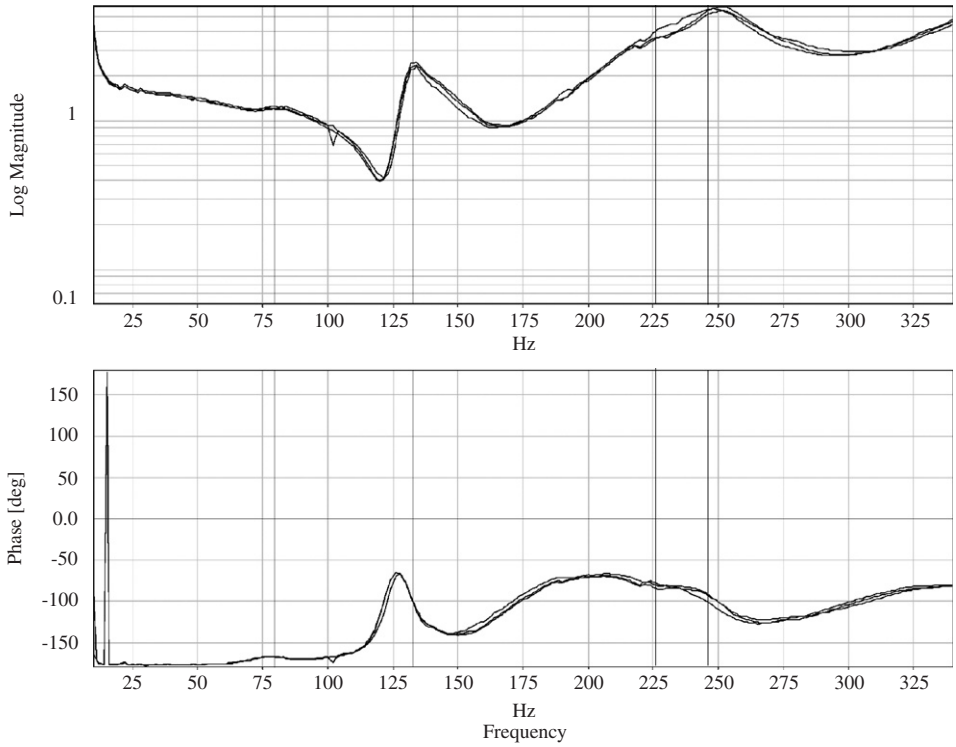

Fig. 2. Frequency response functions at the drive point measured at different times throughout a cadaver experiment. The four vertical lines indicate the frequency of the identified resonances [8].

2. Model

In this section the biodynamic model of the human pelvis is presented.

2.1. Topology

The 18-dof model consists of 3 rigid bodies representing the bones, 12 linear springs representing the ligaments and 8 linear dashpots reproducing the damping effect of the cartilage layer within the joints.

The translation and rotation inertia of the bones are defined in their centers of gravity, both estimated with a CAT-scan based geometrical model of a real pelvis. The rotation inertial properties are expressed in terms of radii of gyration, which are assumed to be determined by the geometry alone. The inertia is therefore solely dependent on the mass.

The disposition of the 12 springs has been chosen to approximate the anatomical ligament configuration, as depicted in Fig. 3 [9]. The number of springs ensures static determination (6 rigid body modes and 12 elastic modes) and excludes mechanisms in the system. The stiffness coefficient of each spring is an independent parameter.

Three non-coplanar dashpots are placed in both sacroiliac joints, to react to all motions except a gliding of the joint interfaces parallel to each other (the fluid between the joint surfaces allows for an almost friction-free gliding). Following kinematic analysis, only two dashpots are placed in the symphysis pubis (due to the system symmetry, a third dashpot in this joint would be redundant). The dashpots of each joint have been assigned the same damping coefficients, for a total of 3 damping parameters to identify.

The model is therefore characterized by 18 parameters: the 3 masses, the 12 stiffness coefficients, and the 3 damping coefficients.

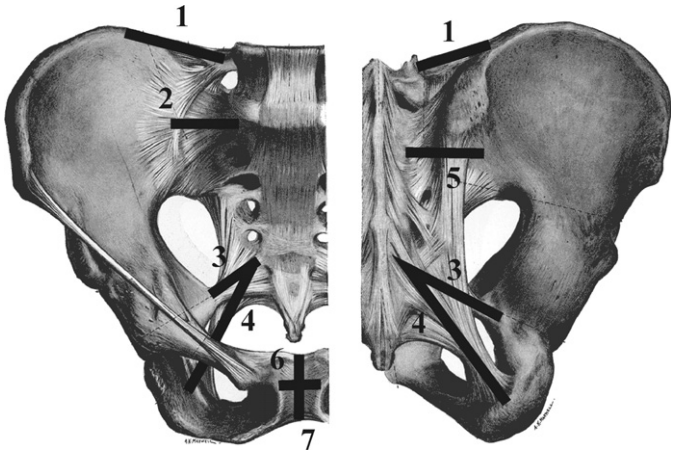

Fig. 3. Anatomy of the human pelvis and its ligamentous system: anterior view (left) and posterior view (right). Added to the figure is the spring configuration in the model. Springs 1–5 are implemented on both left and right side, while springs 6 and 7 are unique. 1: iliolumbar ligament; 2: anterior sacroiliac ligament; 3: sacrospinous ligament; 4: sacrotuberous ligament; 5: posterior sacroiliac ligament; 6: horizontal symphysis pubis ligament; 7: vertical symphysis pubis ligament.

2.2. Parameters

The mass of the 3 rigid bodies has been obtained from the geometrical model by applying a density of $1.92 \times 10^3\,\mathrm{kg/m^3}$ to the material composing the solid. The 12 stiffness coefficients have been estimated using the geometry of the pelvic girdle and published ligament properties [9–11]. The 3 damping coefficients have been set in order to ensure a subcritical damping throughout the frequency range. Due to the symmetry of the system, physical parameters which exist in homologous pairs have been assigned the same values.

The values of the parameters are shown in Table 1.

2.3. Frequency dependency

A linear frequency dependency has been implemented in the stiffness, while an hysteretic component has been added to the viscous damping, according to the harmonic equation of motion in complex form:

$$(-\omega^2 M + \mathrm{j}\omega C + \mathrm{j}D + K + \omega K')\, x = f, \tag{1}$$

where ω is the frequency variable, M, K and C the original system mass, stiffness and damping matrices (as described in Sections 2.1 and 2.2), x the system response harmonic amplitude and f the amplitude of the applied harmonic force. D and K' are defined as:

$$D = f_c C \frac{\omega_{\max}}{4}, \tag{2}$$

$$K' = f_k K \frac{1}{4\ \omega_{\max}}. \tag{3}$$

Here $\omega_{\max}$ represents the maximal frequency in the range of interest, and the factors f_c and f_k allow for a modulation of the dependency for investigation purposes and will be chosen between 0 and 1. At maximal frequency, the elastic and dissipative forces in the case $f_k = f_c = 1$ are 25% bigger than in the case $f_k = f_c = 0$. This frequency dependency has been chosen mild enough to avoid drastic changes in the response of the system.

Table 1
Values of the physical parameters of the model

m_{ili}	m_{sac}	k_{ss}	k_{st}	k_{il}	k_{as}	k_{ps}	k_{ph}	k_{pv}	c_p	c_s
0.61	0.36	1.2e5	0.8e5	1.2e5	15e3	2e5	1e5	5e3	0.8	0.8

m_{ili} and m_{sac}: mass of the ilium (same value left and right) and the sacrum in kg; k_{ss}, k_{st}, k_{il}, k_{as}, k_{ps}, k_{ph} and k_{pv}: stiffness coefficients of, respectively, the sacrospinous, the sacrotuberous, the iliolumbar, the anterior sacroiliac, the posterior sacroiliac (for these 5 same values left and right), the horizontal symphysis pubis and the vertical symphysis pubis ligaments, in N/m; c_p and c_s: damping coefficients of the dashpot groups, respectively, in the symphysis pubis and the sacroiliac joints (same value left and right), in N/(m/s).

3. Identification tools

This section will introduce the two standard modal analysis tools, and the in-house updating algorithm for the identification of the model physical parameters.

Both modal parameters estimation methods considered are in frequency domain. The two main reasons are the high damping present in the human pelvis, and the fact that in the future the experimental data on the pelvis will most probably be obtained with a stepped sine sweep excitation with variable frequency increment. The recent PolyMAX technique proposed in Ref. [12] for advanced modal analysis was not investigated here because it was not available in the commercial codes at our disposal. Given the fact that the PolyMAX method has been shown to exhibit clear stabilization diagrams and superior identification capabilities in some difficult analysis case studies, it would be interesting in future research to test it on data belonging to systems with frequency-dependent mechanical properties.

3.1. Modal analysis tool 1

ME'scopeVES 4.0 (Vibrant Technologies, Inc., USA) is an ensemble of software packages for the post-test analysis of structures' dynamic behaviour. The Visual Modal Pro Package used in this study allows for signal processing and modal analysis.

The modal parameters estimation is achieved by curve-fitting a set of frequency response functions (FRFs). The fitting method can be selected among four. Two methods (the CoQuad and the Peak methods) are single degree of freedom methods, which are used when the resonance peaks are widely separated so that each peak can be treated, in its vicinity, as due to a single mode. These two methods do not give estimates of the damping. To the category of multiple degrees of freedom (mdof) methods belong the polynomial and the complex exponential methods, the first in frequency domain and the latter in time domain, both providing estimates for damping and frequency of the resonances. To maintain a general predictive power of this study we chose to apply a mdof method, and the polynomial method in particular, since the FRFs are already in frequency domain. At any rate, the analysis of one set of simulated data was performed with the complex exponential method and the obtained modal parameters were the same. The polynomial method chosen for this study utilizes the real and imaginary parts of the FRFs for a two-step identification in frequency domain. The FRFs are assumed in the rational fraction form:

$$\alpha(s) = \frac{\sum_{k=0}^{P} a_k s^k}{\sum_{k=0}^{N} b_k s^k}, \tag{4}$$

where $\alpha(s)$ is the transfer function in the Laplace domain, P the number of zeros, N the number of poles, a_k the numerator polynomial coefficients and b_k the denominator polynomial coefficients.

In a first step, the estimates of the frequencies and damping factors, which constitute the poles of the system for all FRFs, are obtained by a nonlinear least-squared error fit of the characteristic polynomials at denominator. The second step foresees a nonlinear least-squared error fit of the polynomial at numerator, for each FRF [13]. The residues are then obtained by a partial fraction expansion of the estimated rational

fraction. Optionally, extra polynomial terms at numerator (a choice from 0 to 8) can be added to compensate for out-of-band modes. For this study, a maximum of 4 extra terms have been allowed to enable compensation while avoiding overfitting.

3.2. Modal analysis tool 2

Structural Dynamics Toolbox SDT (Structural Dynamics Tools, France) is an optimization software for the fitting of a parametric model to measured FRFs through a frequency domain output error minimization [14]. The model implemented in the algorithm is in the partial fraction form:

$$\alpha(s) = \sum_{k=1}^{2N} \frac{R_k}{s - \lambda_k} + E + \frac{F}{s^2}, \tag{5}$$

where $\alpha(s)$ is the transfer function in the Laplace domain, N is the number of modes, λ_k is the pole k, R_k is the residue associated to pole k, and E and F are the residual corrections for modes above, respectively, below the measurement frequency range.

The model in Eq. (5) is a linear function of the residues R_k and residual terms E and F, and a nonlinear function of the poles λ_k. The estimation of the parameters is based on an iterative procedure, which calculates the residues R_k, E and F through linear least-squared error fit having the poles λ_k as parameters, and then uses them to obtain new poles estimates λ_k through a nonlinear optimization. The process is repeated until convergence is reached.

3.3. In-house updating algorithm

The third tool has been developed in the frame of this research and is based on the model of the human pelvis. The squared differences in real and imaginary parts between the measured FRFs and the model-generated FRFs add up to a cost function to be minimized, namely:

$$J(p) = \sum_{k=1}^{N_{\text{samp}}} \sum_{m=1}^{Q} a.\Re\mathfrak{e}(\Delta s_{k,m})^2 + b.\Im\mathfrak{m}(\Delta s_{k,m})^2, \tag{6}$$

$$\Delta s_{k,m} = \alpha_{\text{syn}}(\omega_k, m, p) - \alpha_{\text{meas}}(\omega_k, m), \tag{7}$$

where $J(p)$ is the cost function, p is the parameter set, N_{samp} is the total number of discrete measured frequencies ω_k, Q is the number of measured FRF curves, a and b are real weight factors, α_{syn} is the synthesized FRF, and α_{meas} is the measured FRF.

The parameters tuned during updating are the 3 masses, and the stiffness and damping coefficients. A previous simulation study has shown that the weight factors $a = 1$ and $b = 10$ allow for a good identification [5]. This means a 10-fold weighting of the imaginary part of the squared difference, which forces the algorithm to perform a better fit around the resonance peaks.

3.3.1. Versions A and B

To provide an indication on the effectiveness of the in-house identification and the optimization routines, a version B of the updating algorithm has been created, where the model used for updating includes the additional matrices as in Eq. (1). In this second version, the factors f_k and f_c become parameters to be identified, in addition to the already considered 18 physical parameters. Version A remains the one with constant properties. Results from both versions are presented in this study.

3.3.2. Optimization algorithm

The optimization algorithm to minimize $J(p)$ in Eq. (6) utilizes standard minimization tools. To prevent the convergence to local minima, an automatic routine has been created, which randomly generates one start parameter set at a time within a range of $\pm 10\%$ of the nominal parameters. Starting from this set, a nonlinear least-squared minimum search with fewer frequency points (to keep it computationally cheap) is performed to

determine whether the optimization is converging towards the global minimum. If not, a new set is generated and the optimization attempted again.

The indication for the global minimum is a cost function descending to values smaller than 10^{-13}. This is however only valid in version B, where the model in the algorithm corresponds to the model used to generate the FRFs, and a zero-value optimum exists. In version A, the cost function will not assume zero value at optimum. Therefore, an effective indication of the global minimum is a cost function descending below the value at nominal parameters. The code will keep generating start parameter sets and performing the cheaper minimization mentioned above (with fewer frequency points) until this condition is satisfied. At this point, the optimization with the complete frequency set is started. Convergence is achieved with a termination tolerance on the cost function of 10^{-17}, approximating the zero slope of the minimum.

This termination tolerance on the function value, common to all simulations throughout the study, was first established by performing an optimization on one set of FRFs generated with no frequency dependency but polluted with noise. Different termination tolerances were tried until all 18 parameters showed an error $<1\%$. The noise added to the FRFs was Gaussian additive white noise in frequency domain [15]:

$$\alpha_{\text{noise}}(\omega_k, m) = \alpha(\omega_k, m) + g n_n e^{j2\pi n_u}, \tag{8}$$

where $\alpha_{\text{noise}}(\omega_k, m)$ is the polluted mth FRF (receptance) at frequency ω_k, $\alpha(\omega_k, m)$ the generated mth FRF at frequency ω_k, g a constant, n_n a normally distributed random number with mean value 0 and standard deviation 1, and n_u a random number uniformly distributed between 0 and 1. The value of g was set as 5×10^{-6} times the maximal amplitude present in all FRFs. The noise-polluted drive point FRF is illustrated in Fig. 4.

4. Simulations

In this section the procedure related to the generation of the data, their utilization in the software tools and the evaluation criteria for their identification capability will be explained.

4.1. Data synthetization

To avoid problems arising by modes with zero frequency (rigid body modes), the diagonal terms of the stiffness matrix corresponding to the 6 dofs of the sacrum were increased by 1%. This corresponds to attaching the sacrum to the environment with springs 100 times less stiff than the joints. The system response was synthesized by solving the equation of motion (1) in the frequency range 0–550 Hz (encompassing all the

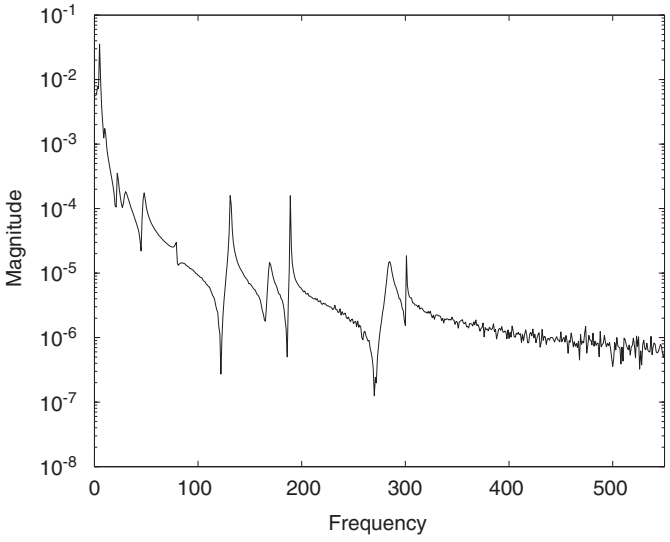

Fig. 4. Magnitude of the drive point receptance FRF between 0 and 550 Hz with additive Gaussian white noise.

resonances) for a harmonic force applied on the left ilium. The solution was transformed in receptance at nine points on the pelvis (three per bone), plus the drive point, for a total of 28 FRFs. Fig. 5 shows the measurement and excitation points.

For both modal analysis tools a frequency discretization of 0.05 Hz was chosen to maximize the information content. For the in-house updating algorithm a much coarser discretization had to be chosen for computational cost reasons. For the optimization screening, data points were generated every 50 Hz (for a total of 12 points), while for the actual optimization the frequency increment was of 10 Hz (for a total of 56 data points). A finer discretization of 5 Hz increased considerably the computation time but did not improve the identification results.

The investigation on the effects of frequency dependency was modulated with the factors f_k and f_c, as presented in Eqs. (2) and (3)) in Section 2. Seven combinations of f_k and f_c have been considered, as indicated in Table 2.

4.2. Determination of the theoretical values

The theoretical modal parameters were obtained by solving the eigenproblem in state space. In the case of constant system matrices ($f_c = f_k = 0$) a numerical solution was directly obtained. In the case of frequency-dependent system matrices the eigenproblem was solved for each mode by a fixed point iteration scheme, as explained in this section.

The state space matrices A and B were defined as

$$A_i = \begin{bmatrix} -M & 0 \\ 0 & K + K'\omega_{r,i} \end{bmatrix}, \tag{9}$$

$$B_i = \begin{bmatrix} 0 & M \\ M & C + \dfrac{D}{\omega_{r,i}} \end{bmatrix}, \tag{10}$$

where $\omega_{r,i}$ is the damped resonance frequency of mode r at the ith iteration step.

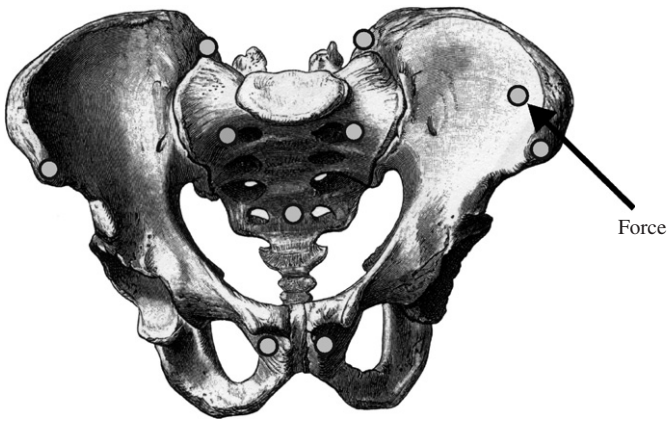

Fig. 5. Nine points of measurement on the pelvis, and location and orientation of the excitation on the left ilium.

Table 2
Cases considered for the study

Case	1	2	3	4	5	6	7
f_k	0	0	0	0.5	1	0.5	1
f_c	0	0.5	1	0	0	0.5	1

The eigenproblem in state-space was solved at each step i with the frequency-dependent matrices as expressed in Eqs. (9) and (10). The absolute value of the imaginary part of the obtained pole $\lambda_{r,i+1} = -\sigma_{r,i+1} \pm j\omega_{r,i+1}$ was then used to update the matrices A_i and B_i into A_{i+1} and B_{i+1}, and the eigenproblem solved again. This iterative procedure was performed until convergence was reached. In mathematical form:

$$\text{solve} \quad (\lambda_{r,i+1}B_i + A_i)\theta_{r,i+1} = 0 \text{ for } \lambda_{r,i+1},\ \theta_{r,i+1}, \tag{11}$$

$$\omega_{r,i+1} = |\Im\mathfrak{m}(\lambda_{r,i+1})|, \tag{12}$$

$$\sigma_{r,i+1} = -\Re\mathfrak{e}(\lambda_{r,i+1}), \tag{13}$$

$$\text{until} \quad \frac{|\omega_{r,i+1} - \omega_{r,i}|}{\omega_{r,i+1}} < 10^{-6} \quad \text{and} \quad \frac{|\sigma_{r,i+1} - \sigma_{r,i}|}{\sigma_{r,i+1}} < 10^{-6}. \tag{14}$$

Here $\lambda_{r,i+1} = -\sigma_{r,i+1} \pm j\omega_{r,i+1}$ is the pole r of the system at the $i+1$th iteration step, and θ_{i+1} is the mode shape for mode r at the $i+1$th iteration step. The cut-off value of 10^{-6} is the relative error in frequency and damping factor and is deemed sufficiently small.

The actual mode shape is the one associated to the converged eigenvalue. The damping ratio was calculated from the converged λ_r, for each mode r:

$$\zeta_r = \frac{\sigma_r}{\sqrt{\omega_r^2 + \sigma_r^2}}. \tag{15}$$

The theoretical resonance frequencies and damping ratios are given in Tables 3 and 4.

4.3. Evaluation of the identification

The identified modal parameters were compared to the theoretical parameters. In the case of the in-house updating algorithm, comparison was performed between the physical parameters. In addition, the model

Table 3
Theoretical resonance frequencies in Hz for the different cases

$f_k = 0$ $f_c = 0$	$f_k = 0$ $f_c = 0.5$	$f_k = 0$ $f_c = 1$	$f_k = 0.5$ $f_c = 0$	$f_k = 1$ $f_c = 0$	$f_k = 0.5$ $f_c = 0.5$	$f_k = 1$ $f_c = 1$
2.96	2.96	2.96	2.96	2.96	2.96	2.97
3.77	3.77	3.77	3.77	3.77	3.77	3.77
4.71	4.71	4.73	4.71	4.71	4.72	4.73
6.90	6.90	6.90	6.90	6.91	6.90	6.91
8.86	8.86	8.86	8.87	8.88	8.87	8.88
9.45	9.45	9.47	9.46	9.47	9.46	9.49
20.88	20.87	20.87	20.93	20.98	20.92	20.97
27.82	27.83	27.87	27.90	27.99	27.92	28.04
43.20	43.20	43.21	43.41	43.62	43.41	43.63
46.16	46.12	46.04	46.40	46.64	46.36	46.53
76.91	76.91	76.91	77.59	78.27	77.59	78.26
126.69	126.69	126.69	128.53	130.39	128.53	130.39
161.69	161.69	161.70	164.69	167.74	164.69	167.75
180.55	180.55	180.55	184.29	188.11	184.29	188.11
264.18	264.18	264.18	272.23	280.52	272.23	280.51
266.80	266.79	266.78	275.01	283.47	275.00	283.45
281.27	281.26	281.26	290.40	299.82	290.40	299.81
393.30	393.30	393.30	411.27	430.02	411.27	430.02

Table 4
Theoretical damping ratios in % for the different cases

$f_k = 0$ $f_c = 0$	$f_k = 0$ $f_c = 0.5$	$f_k = 0$ $f_c = 1$	$f_k = 0.5$ $f_c = 0$	$f_k = 1$ $f_c = 0$	$f_k = 0.5$ $f_c = 0.5$	$f_k = 1$ $f_c = 1$
0.02	0.38	0.73	0.02	0.02	0.37	0.73
0.01	0.19	0.38	0.01	0.01	0.19	0.38
0.08	1.17	2.19	0.08	0.08	1.17	2.18
0.00	0.03	0.06	0.00	0.00	0.03	0.06
0.04	0.34	0.63	0.04	0.04	0.34	0.63
0.09	0.72	1.33	0.09	0.09	0.72	1.33
0.43	1.83	3.23	0.42	0.42	1.82	3.20
1.27	4.42	7.60	1.27	1.26	4.40	7.51
0.41	1.08	1.74	0.41	0.41	1.07	1.71
0.63	1.57	2.51	0.63	0.62	1.56	2.46
0.32	0.60	0.89	0.32	0.31	0.60	0.86
0.03	0.04	0.06	0.03	0.03	0.04	0.06
0.48	0.68	0.89	0.47	0.46	0.67	0.84
0.01	0.01	0.01	0.01	0.01	0.01	0.01
0.51	0.65	0.78	0.50	0.48	0.63	0.72
0.46	0.58	0.70	0.45	0.44	0.56	0.65
0.03	0.04	0.05	0.03	0.03	0.04	0.05
0.07	0.08	0.10	0.07	0.07	0.08	0.09

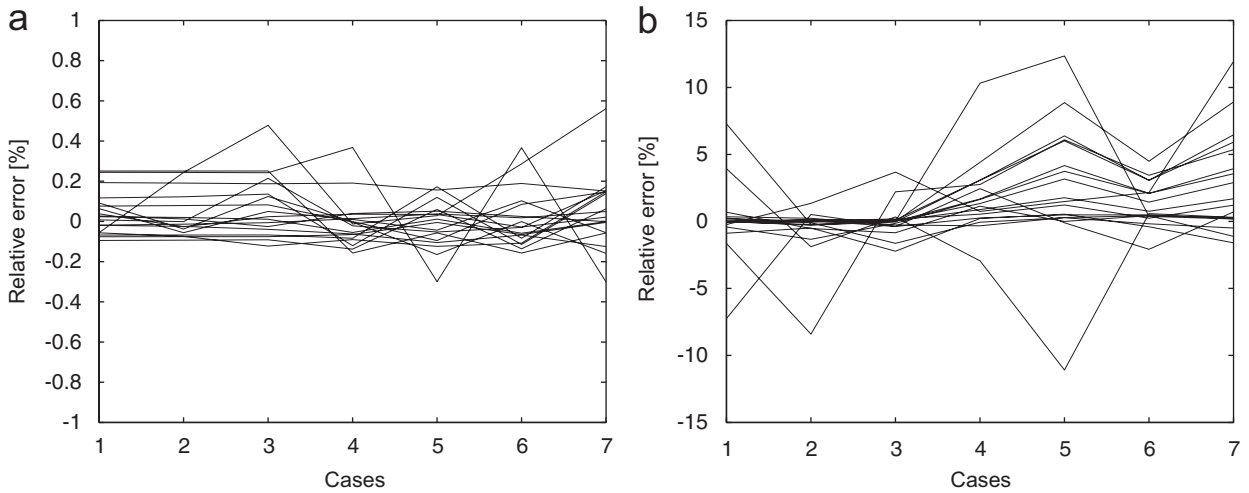

Fig. 6. ME'scope: relative estimation error in %: (a) in frequency, (b) in damping ratio. Each line connects the error related to the same mode throughout the cases, for the 18 modes. Numbered from 1 to 7 in the x-axis are the considered cases: (1) $f_k = 0, f_c = 0$, (2) $f_k = 0, f_c = 0.5$, (3) $f_k = 0, f_c = 1$, (4) $f_k = 0.5, f_c = 0$, (5) $f_k = 1, f_c = 0$, (6) $f_k = 0.5, f_c = 0.5$, (7) $f_k = 1, f_c = 1$.

updated with the identified parameters was used to compute the frequencies and modes as explained in Section 4.2, allowing for a comparison in modal space. The results will be presented in the next section.

5. Identification results

In this section the results of the comparison between the theoretical values and the identified values are given. The errors in resonance frequencies and damping ratios, and the Modal Assurance Criterion, are provided in graphical form.

5.1. Modal analysis tool 1

ME'scope was able to identify the frequencies very well, with errors ranging between −0.4% and +0.6% (Fig. 6a). The damping ratio proved to be more challenging, with mode 2 showing the maximal error of +13% (Fig. 6b). The mode shapes were generally very well identified (MAC > 0.95) with the exceptions of modes 15 and 18, which were increasingly difficult with increasing f_c (Fig. 7). Going from $f_c = 0$ to $f_c = 0.5$ to $f_c = 1$, their MAC values plummeted from 0.9 to 0.63 to 0.4.

5.2. Modal analysis tool 2

SDT performed comparably well in the estimation of the frequencies (Fig. 8a). The errors for modes 6, 7, 8, 9 and 10 increased with increasing f_c, independently from the value of f_k. The maximal error, for mode 8, reached

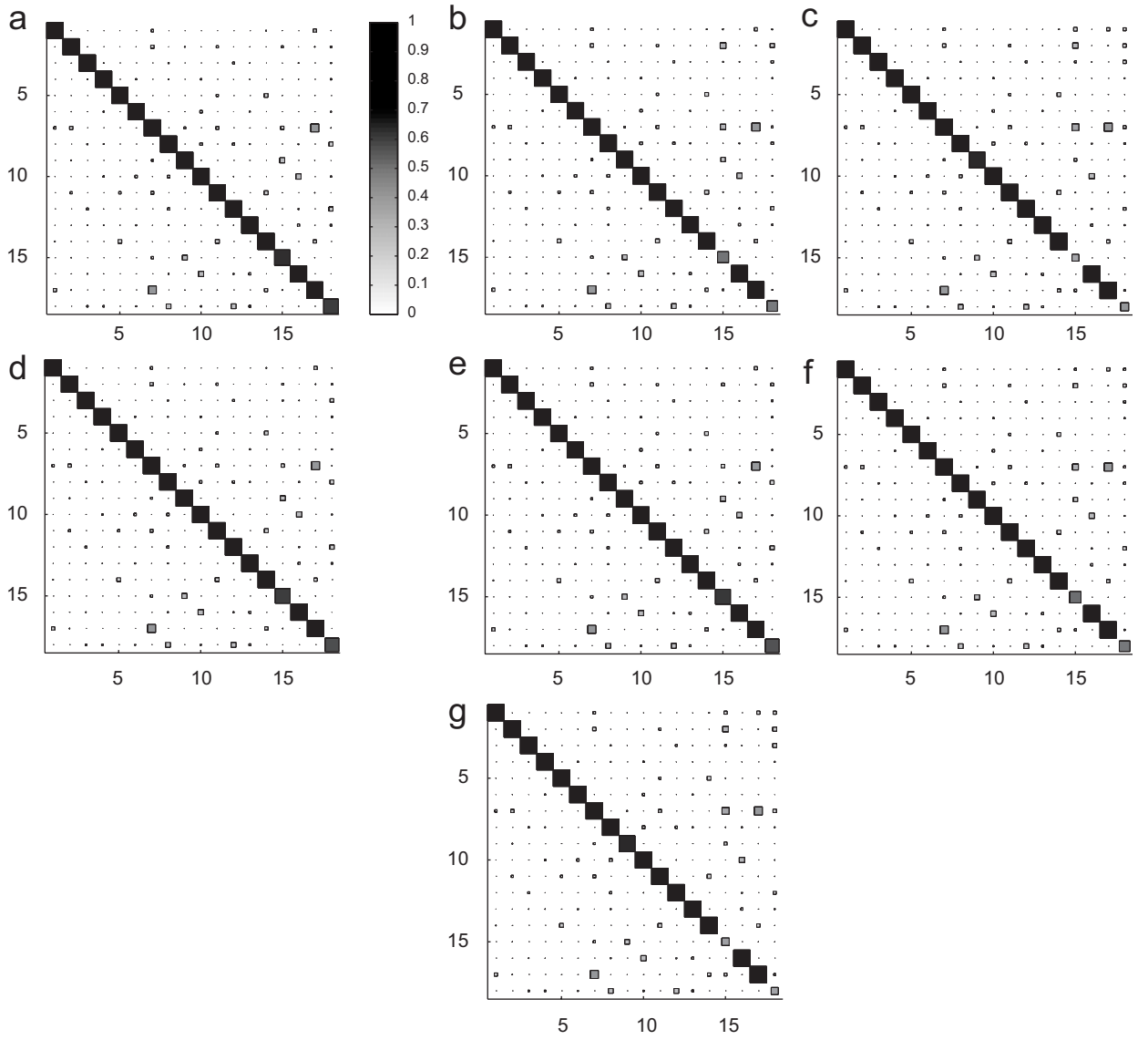

Fig. 7. ME'scope: MAC values between the theoretical and the identified mode shapes for the 7 considered cases: (a) $f_k = 0, f_c = 0$, (b) $f_k = 0, f_c = 0.5$, (c) $f_k = 0, f_c = 1$, (d) $f_k = 0.5, f_c = 0$, (e) $f_k = 1, f_c = 0$, (f) $f_k = 0.5, f_c = 0.5$, (g) $f_k = 1, f_c = 1$.

0.75% for $f_c = 1$. The errors in damping ratio seemed to be dependent mostly on the factor f_k (Fig. 8b). Modes 8 through 18 showed an error which increased in sequence with the modes themselves. The maximal error was seen for mode 18 at $f_k = 1$, and it reached 9%. The mode shapes were very well identified. The MAC values for the worst case scenario $f_c = 1$ and $f_k = 1$ were all >0.99 except mode 10, for which the value was 0.94 (Fig. 9).

5.3. Updating algorithm version A

The frequency estimation error grew from zero at $f_k = 0, f_c = 0$ to $\pm 3\%$ at $f_k = 0, f_c = 1$, with the exception of mode 9, which reached already 5% at $f_k = 0, f_c = 0.5$ (Fig. 10a). The results got generally worse with increasing f_k, with mode 9 remaining around $+5\%$ and mode 10 peaking to 35% at $f_k = 1, f_c = 1$. The damping ratio estimation was badly performed (Fig. 10b). Errors were distributed in the range -100% to $+400\%$.

The physical parameters explained the poor identification of the damping: the errors in the two damping coefficients of the sacroiliac joints reached values between $+300$ and $+500\%$ for $f_c = 0.5$ and $f_c = 1$, independently from f_k. The other parameters showed errors distributed in the range $\pm 30\%$ (Fig. 10c). The mode shape estimation showed switching between modes 9 and 10, and 15 and 16. No direct relation was seen between the occurrence of the switching and the factors f_k and f_c (Fig. 11).

5.4. Updating algorithm version B

Even though a successful identification was expected in all cases for the modified algorithm B, the routine could not find the global minimum for cases 5 and 7 (characterized by $f_k = 1$): the optimization screening was interrupted after 2000 unsuccessful trials. In all other cases the algorithm performed perfectly. The relative error in resonance frequency did not exceed $\pm 0.01\%$, the error in damping ratio did not exceed $\pm 0.5\%$, and the error in the physical parameters did not exceed $\pm 0.5\%$. The MAC values reflected the quality of the identification and showed perfect mode shape correlation. The provision of the individual results is deemed unnecessary due to the clarity of such results.

6. Discussion

Both standard modal analysis tools performed well in estimating the resonance frequencies. The damping estimations were sensibly better with SDT, and the errors showed, in contrast to ME'scope, the existence of a

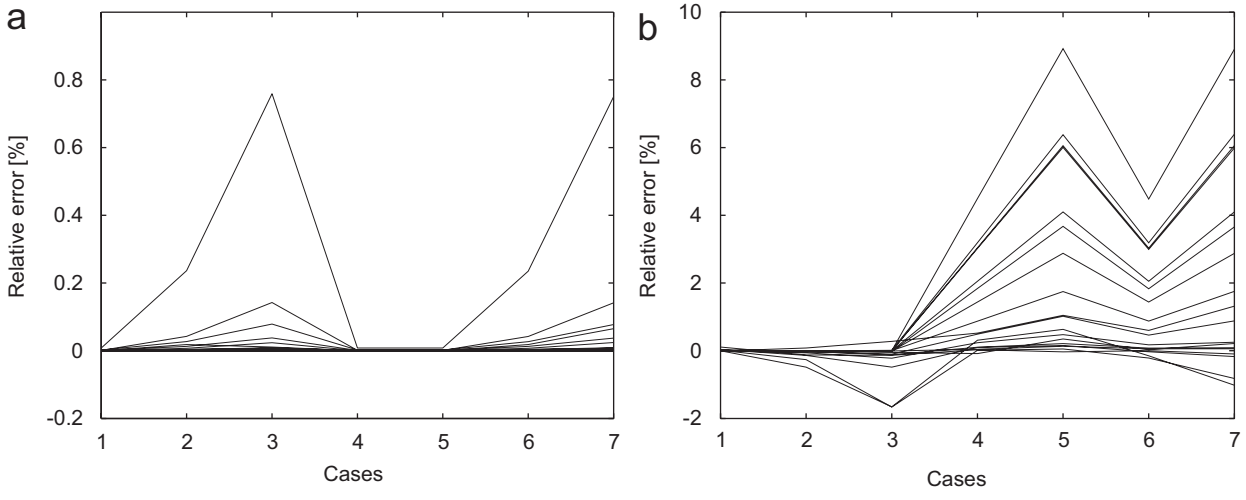

Fig. 8. SDT: relative estimation error in %: (a) in frequency, (b) in damping ratio. Each line connects the error related to the same mode throughout the cases, for the 18 modes. Numbered from 1 to 7 in the x-axis are the considered cases: (1) $f_k = 0, f_c = 0$, (2) $f_k = 0, f_c = 0.5$, (3) $f_k = 0, f_c = 1$, (4) $f_k = 0.5, f_c = 0$, (5) $f_k = 1, f_c = 0$, (6) $f_k = 0.5, f_c = 0.5$, (7) $f_k = 1, f_c = 1$.

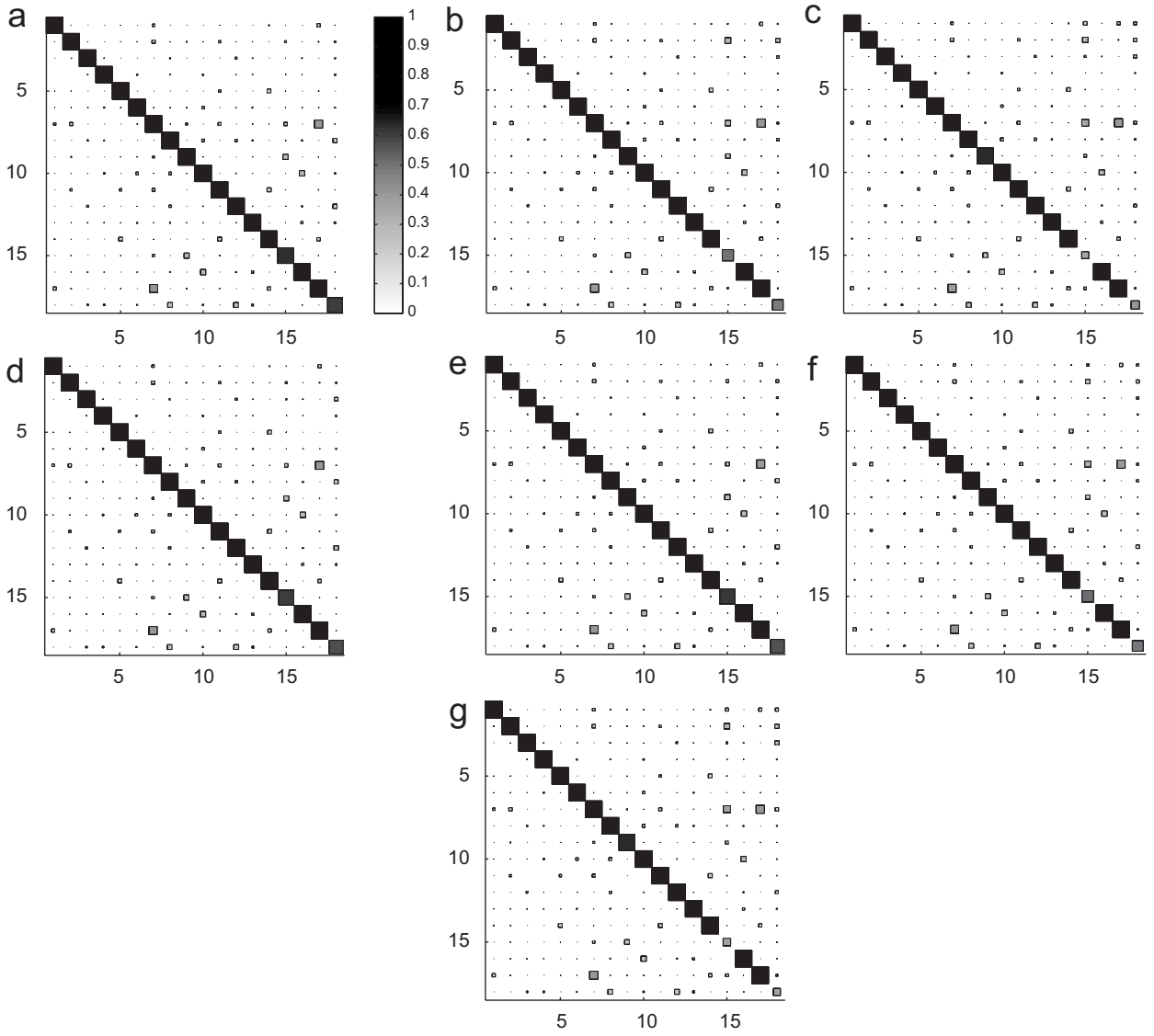

Fig. 9. SDT: MAC values between the theoretical and the identified mode shapes for the 7 considered cases: (a) $f_k = 0, f_c = 0$, (b) $f_k = 0, f_c = 0.5$, (c) $f_k = 0, f_c = 1$, (d) $f_k = 0.5, f_c = 0$, (e) $f_k = 1, f_c = 0$, (f) $f_k = 0.5, f_c = 0.5$, (g) $f_k = 1, f_c = 1$.

pattern, which is remarkable when considering the level of user interaction allowed during the analysis. The tendency seemed to indicate that the higher the frequency of the mode, the more difficult the estimation of its damping. A possible explanation for this is that for a given damping ratio the peak is broader for modes at higher frequency. A frequency-dependent damping has therefore a more important impact on the immediate surroundings of the peak, influencing its identification.

SDT performed better in the identification of the mode shapes than ME'scope, which encountered difficulties in estimating mode shapes 15 and 18. An explanation lies in their visibility. Mode 15 was often shadowed by mode 16, which lay a few Hz higher. Mode 18 was clearly visible only on few of the 28 FRFs, and in some it was not visible at all.

It can be noted that not all the off-diagonal values of the MAC are zero, and appear almost unchanged in all graphs. In fact, they are present also when calculating the MAC values within the theoretical mode shapes themselves.

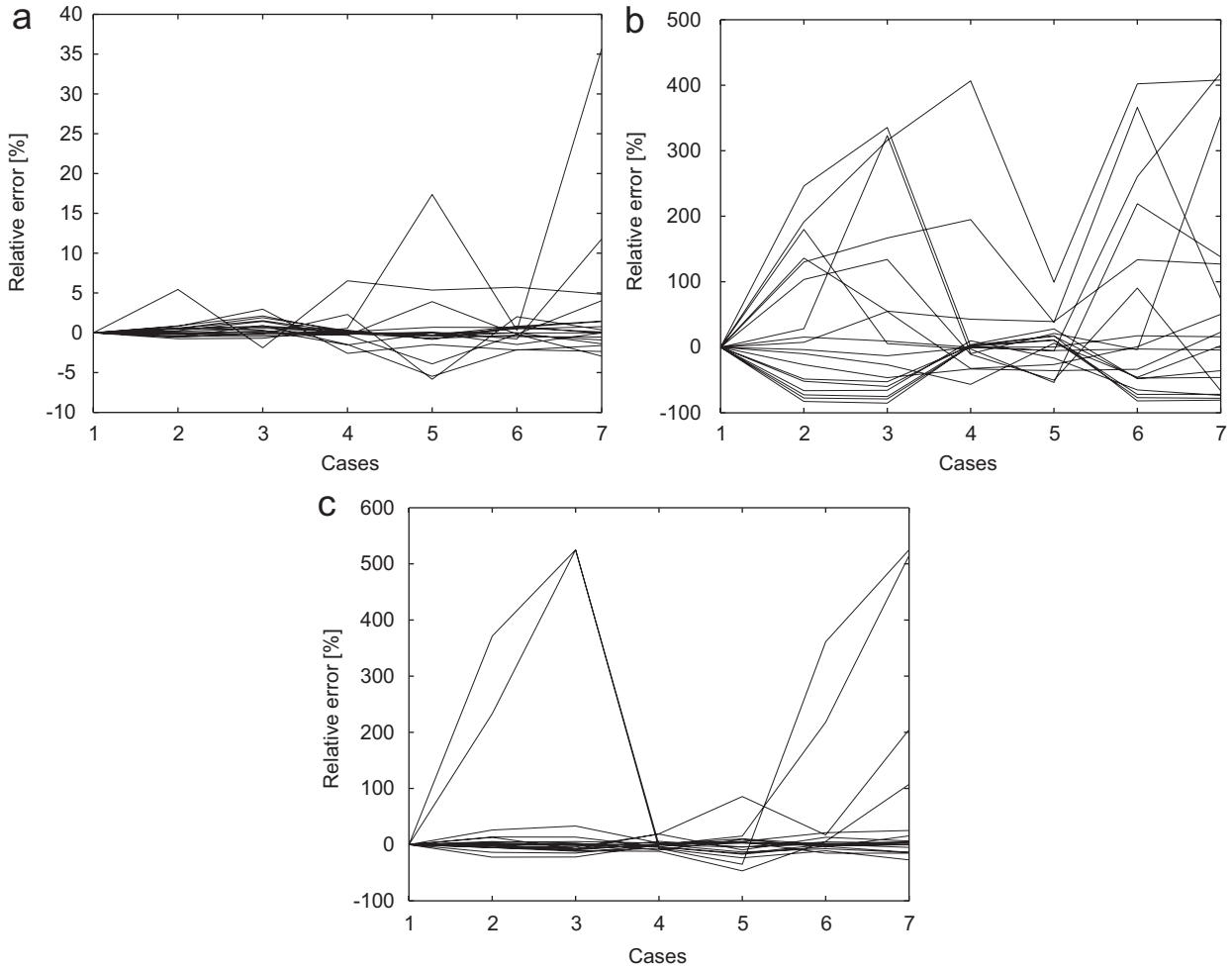

Fig. 10. Updating algorithm A: relative estimation error in %: (a) in frequency, (b) in damping ratio, (c) in system parameters. Each line in panels (a) and (b) connects the error related to the same mode throughout the cases, for the 18 modes. In panel (c) the lines connect the 18 parameters of the model as defined in Section 2.1. The two parameters showing the highest errors in panel (c) in cases (2), (3), (6) and (7) are the left and right c_s. Numbered from 1 to 7 in the x-axis are the considered cases: (1) $f_k = 0, f_c = 0$, (2) $f_k = 0, f_c = 0.5$, (3) $f_k = 0, f_c = 1$, (4) $f_k = 0.5, f_c = 0$, (5) $f_k = 1, f_c = 0$, (6) $f_k = 0.5, f_c = 0.5$, (7) $f_k = 1, f_c = 1$.

The updating algorithm version A showed a high sensitivity to frequency dependencies. The damping ratios seemed to suffer the most from the uncorrect estimation of the physical parameter, and certainly reflected the large errors in the damping coefficients identification. The frequency estimation was less dramatic, even though poor. The mode switching occurring between modes 9 and 10 and modes 15 and 16 can be explained by their respective proximity. Both pairs lie within few Hz from each other, as shown in Table 3. In fact in cases 2 and 4 (Fig. 11b and d, corresponding to $f_k = 0, f_c = 0.5$ and $f_k = 0.5, f_c = 0$) the estimated parameters produced modes 9 and 10 with very close frequencies (45.549 and 45.772 Hz in case 2, and 46.242 and 46.661 Hz in case 4). A ''numerical'' switching cannot be ruled out.

The difficulties encountered by this method can be interpreted by considering the absence of user interaction: in its present form it does not allow for a preliminary localization of the peaks, and it is therefore less able to compensate for peak shifts.

The updating algorithm version B, however, even though theoretically provided with all the information to perform a perfect estimation, could not always overcome the problem of the local minima. The two failed optimizations were tried again by reducing the range where the start parameter sets were randomly picked, from $\pm 10\%$ to $\pm 1\%$. In the case of $f_k = 1$, $f_c = 0$, the initial screening provided a valid start set after 7 trials,

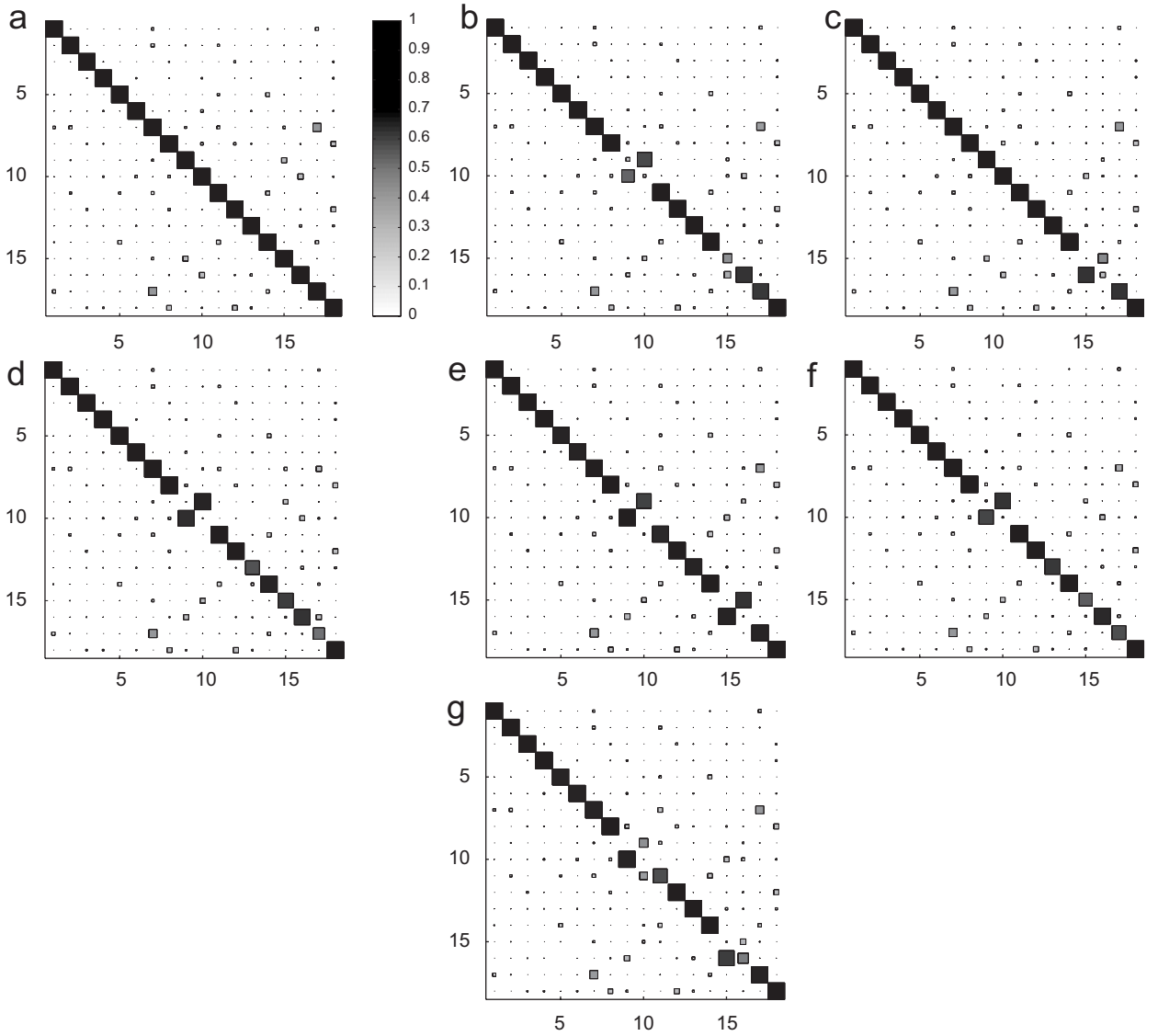

Fig. 11. MAC values between the theoretical and the mode shapes estimated with the updating algorithm A for the 7 considered cases: (a) $f_k = 0, f_c = 0$, (b) $f_k = 0, f_c = 0.5$, (c) $f_k = 0, f_c = 1$, (d) $f_k = 0.5, f_c = 0$, (e) $f_k = 1, f_c = 0$, (f) $f_k = 0.5, f_c = 0.5$, (g) $f_k = 1, f_c = 1$.

while in the case of $f_k = 1$, $f_c = 1$ it cost 366 trials. One more simulation showed that the algorithm was able to perform the identification under normal circumstances with $f_k = 0.9$, $f_c = 0$. All identifications were perfect.

These results suggest that there are local minima very close to the global minimum. One-dimensional visualization of the cost function is obtained by fixing all parameters but one at their nominal values, and sweeping the variable parameter from -20% to $+20\%$ of its nominal value. The presence of local minima is confirmed at $f_k = 1$ and $f_c = 1$ for the parameters m_{ili}, m_{sac}, k_{il}, and k_{ps}, as shown in Fig. 12. The other parameters induce a concave cost function. The shape of the cost function remains very similar also when changing the ratio between a and b. The difficulties shown by version B seem to be due to its optimization algorithm more than to the definition of the cost function. The effort of devising a more sophisticated global minimum search is worthwhile, since the advantage of this algorithm over the modal analysis tools is that, being specific for the pelvis model, it allows for a direct identification of its physical parameters.

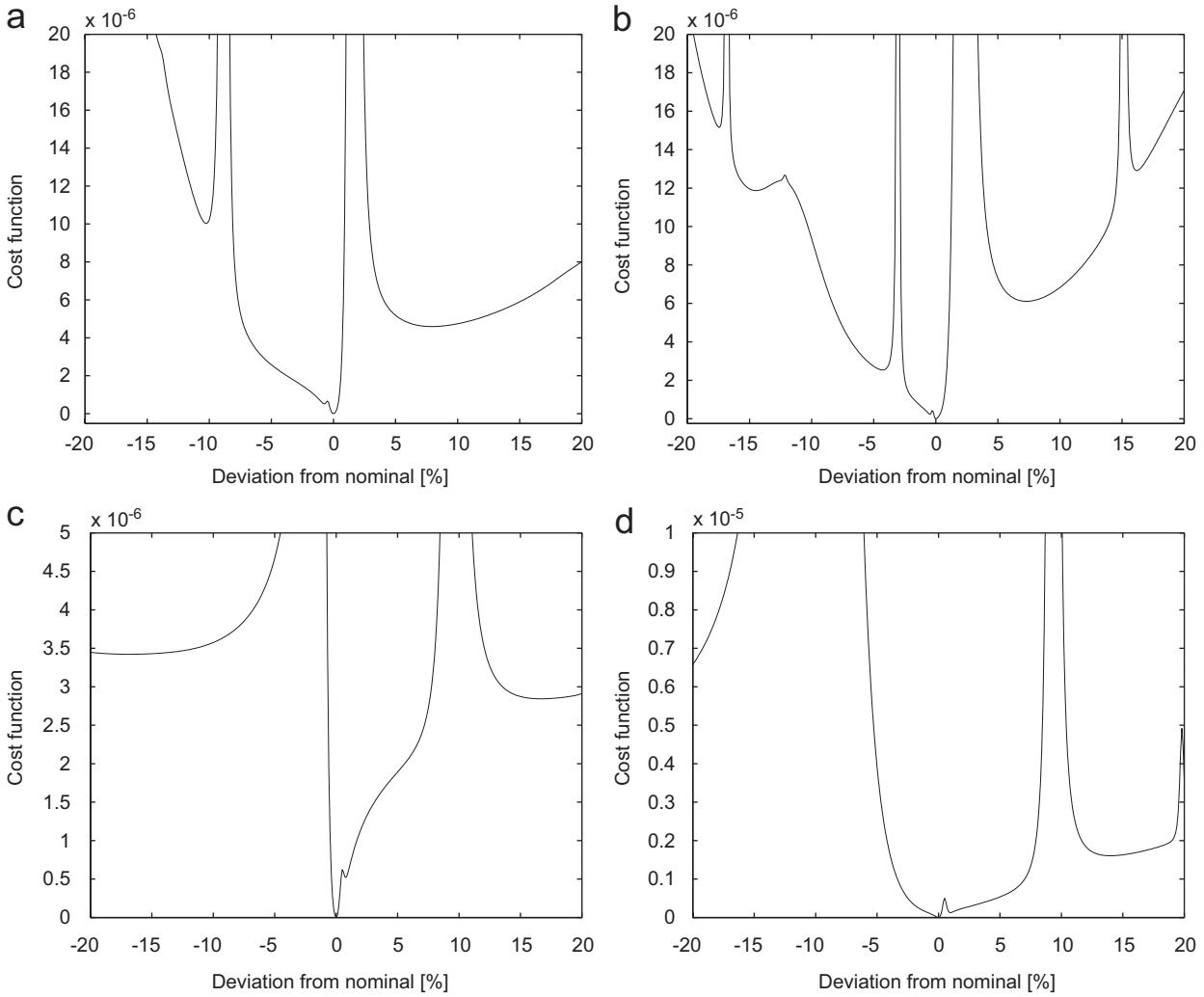

Fig. 12. Cost function value (version B) obtained by fixing all parameters but one at the nominal value and letting the variable one sweep from −20% to +20% (x-axis): (a) mass of the ilium, (b) mass of the sacrum, (c) stiffness coefficient of the iliolumbar ligament, (d) stiffness coefficient of the posterior sacroiliac ligament. The factors of dependency are $f_k = 1$ and $f_c = 1$.

The simulated data shown in Fig. 4 present characteristics which are easier to identify (lower damping) than the real *in vitro* test data shown in Fig. 2. Higher damping values could not be implemented in order to maintain a subcritical damping at all frequencies, as explained in Section 2.2. The difficulties encountered in this study by the investigated tools would probably be aggravated should real frequency-dependent data be used, which are comparable to the strongly damped cadaver response data.

7. Conclusions

In this study the effects of frequency-dependent properties on the identification of system parameters has been investigated. Two standard modal analysis tools and one in-house updating algorithm in frequency domain have been used. While resonance frequencies were well identified by the two modal analysis tools (with relative errors lower than 1%), the damping proved to be more problematic (errors in the order of magnitude of 10%). The identification of the mode shapes was good, even though one modal analysis tool had difficulties identifying mode shapes when their frequencies were close to each other. The in-house updating algorithm with no built-in frequency dependency performed worse, especially in the damping estimation. Most

frequencies were estimated within ±15% error, with some frequencies peaking to 35%. The error in damping ratio reached values of 400%. The performance in estimating the mode shapes was generally good, with the presence of mode switching for closely spaced modes. Implementation of the frequency dependency in the updating algorithm, on the other hand, allowed for a perfect system identification, even though in some cases the identification was compromised by the presence of local minima very close to the global minimum.

Acknowledgements

This study was performed in the frame of the project "Ultrasound vibration measurements for the detection of musculoskeletal disorders" (RPG. 5289), financially supported by the Dutch funding agency for university research, the Technology Foundation STW, Utrecht, The Netherlands (www.stw.nl).

References

[1] C. Snijders, A. Vleeming, R. Stoeckart, Transfer of lumbosacral load to iliac bones and legs: part 1: biomechanics of self-bracing of the sacroiliac joints and its significance for treatment and exercise, *Clinical Biomechanics* 8 (6) (1993) 285–294.
[2] L. Damen, Laxity Measurements of the Sacroiliac Joints in Women with Pregnancy-related Pelvic Pain, PhD Thesis, Erasmus University Rotterdam, 2002.
[3] E. Vlaanderen, N. Conza, C. Snijders, A. Bouakaz, N. de Jong, Low back pain, the stiffness of the sacroiliac joint: a new method using ultrasound, *Ultrasound in Medicine and Biology* 31 (1) (2005) 39–44.
[4] N. Conza, A. Soethoudt, E. Vlaanderen, D. Rixen, In vivo bone vibration measurement by ultrasound, *24th International Modal Analysis Conference (IMAC XXIV)*, Society for Experimental Mechanics, St. Louis, MO, USA, 2006.
[5] N. Conza, D. Rixen, Biodynamical parameter estimation using frequency domain updating, *23rd International Modal Analysis Conference (IMAC XXIII)*, Society for Experimental Mechanics, Orlando, FL, USA, 2005.
[6] P. Provenzano, R. Lakes, D. Corr, R. Vanderby, Application of nonlinear viscoelastic models to describe ligament behavior, *Biomechanics and Modeling in Mechanobiology* 1 (1) (2002) 45–57.
[7] N. Conza, D. Rixen, Dynamical experiments on human pelvises: challenges and preliminary results, *23rd International Modal Analysis Conference (IMAC XXIII)*, Society for Experimental Mechanics, Orlando, FL, USA, 2005.
[8] N. Conza, D. Rixen, Vibration testing of a fresh-frozen human pelvis: the role of the pelvic ligaments, *Journal of Biomechanics*, in press, doi:10.1016/j.jbiomech.2006.07.001.
[9] H. Gray, *Anatomy of the Human Body*, 20th ed., Lea & Febiger, Philadelphia, 1918.
[10] Y. Fung, *Biomechanics. Mechanical Properties of Living Tissues*, second ed., Springer, New York, 1993.
[11] J. Black, G. Hastings (Eds.), *Handbook of Biomaterial Properties*, first ed., Chapman & Hall, London, 1998.
[12] P. Guillaume, P. Verboven, S. Vanlanduit, H.V.D. Auweraer, B. Peeters, A poly-reference implementation of the least-squares complex frequency-domain estimator, *21st International Modal Analysis Conference (IMAC XXI)*, Society for Experimental Mechanics, Kissimmee, FL, USA, 2003.
[13] M. Richardson, D. Formenti, Global curve fitting of frequency response measurements using the rational fraction polynomial method, *3rd International Modal Analysis Conference (IMAC III)*, Society for Experimental Mechanics, Orlando, FL, USA, 1985.
[14] E. Balmès, Frequency domain identification of structural dynamics using the pole/residue parametrization, *14th International Modal Analysis Conference (IMAC XIV)*, Society for Experimental Mechanics, Dearborn, MI, USA, 1996.
[15] A. Thite, D. Thompson, The quantification of structure-borne transmission paths by inverse methods. part 1: improved singular value rejection methods, *Journal of Sound and Vibration* 264 (2) (2003) 411–431.